



# Investigations on structural, optical and magnetic properties of Fe and Dy co-doped ZnO nanoparticles

Jaskaran Singh Malhotra<sup>1</sup> · Arun Kumar Singh<sup>2</sup> · Robin Khosla<sup>3</sup> · Satinder Kumar Sharma<sup>3</sup> · Gyaneshwar Sharma<sup>4</sup> · Sanjeev Kumar<sup>4</sup>

Received: 21 October 2017 / Accepted: 23 November 2017 / Published online: 5 December 2017  
© Springer Science+Business Media, LLC, part of Springer Nature 2017

## Abstract

ZnO nanoparticles doped with dysprosium (Dy) were synthesized using sol–gel method. Further iron (Fe) doping was done to study the effect on structural, optical and magnetic properties of Dy doped ZnO nanoparticles. X-ray diffraction studies show a minor change in lattice parameters with no impurity phase. Raman studies also show no change in the hexagonal structure of ZnO with Fe and Dy co-doping. Photoluminescence at room temperature shows the presence of defects which further decreases with increase in Fe co-doping. Dy doped ZnO nanoparticles illustrate the combination of paramagnetic and weak ferromagnetic behavior. Further, increase in Fe co-doping in 2% Dy doped ZnO leads to antiferromagnetic behavior.

## 1 Introduction

Dilute magnetic semiconductors (DMSs) based ‘Spintronics’ is a promising technology for designing of innovative solid state devices [1]. It exploits the combination of fundamental charge on the electron with the intrinsic spin of the electron [2]. Various demanding applications like quantum computing, highly sensitive magnetic sensors, data storage, etc. can be possible through spintronics based technology because spin manipulation can be done easily by the application of an external magnetic field. Spintronics based technology will boost up by getting DMS materials with high magnetization. Worldwide, various groups are actively involved in achieving ferromagnetism at room temperature (RTFM) in wide band gap semiconductors [3–5] like ZnO, GaAs, GaN, etc.

Among various DMS materials, ZnO is still attractive because of its direct wide bandgap (3.37 eV) and large exciton energy (60 meV) [6]. Further non-toxic nature,

chemical stability towards air, inexpensiveness and relative abundance, makes ZnO an interesting material for versatile applications [7]. In addition, high thermal conductivity and high refractive index make ZnO suitable for antibacterial and UV-protection studies [8].

Diamagnetic and paramagnetic behaviors of ZnO at room temperature are the major shortcomings for their use in novel magneto-optical applications. RTFM resulting through vacancy mediation has been reported in ZnO systems [9–11]. Various groups are working to improve the RTFM in ZnO by replacing the host Zn atom by transition metal and rare earth dopants. It is well reported that RTFM in transition metal doped ZnO results due to the *d–d* exchange coupling among non localized and exterior *3d* electron of transition metal [12–15]. Often zero orbital momentum of *3d* electron in transition metal consequences due to its non-localization. Rare earth ion doping results in stronger magnetization in comparison to transition metals due to indirect exchange interaction of *4f* electron via *5d* or *6s* conduction electrons [16–19].

Recently, concurrent doping of two transition metals showed an increase in magnetization. Enhancement in ferromagnetism is reported in Ni and Co co-doped ZnO and suggested that the increase in carrier concentration results in such behavior [20]. Similar behavior was observed in Al and Cu co-doped ZnO rods [21] and Al and Fe co-doped ZnO thin films [22]. Recently, rare earth doping jointly with the transition metal in ZnO has been vigorously explored. Xu et al. [23] investigated RTFM in Nd and Mn co-doped ZnO

✉ Sanjeev Kumar  
sanjeev04101977@gmail.com

<sup>1</sup> Mechanical Engineering Department, PEC University of Technology, Chandigarh 160012, India

<sup>2</sup> Electronics and Communications Engineering Department, PEC University of Technology, Chandigarh 160012, India

<sup>3</sup> School of Computing and Electrical Engineering, Indian Institute of Technology, Mandi 175005, India

<sup>4</sup> Applied Sciences Department, PEC University of Technology, Chandigarh 160012, India

films. Photongkam et al. [24] and Assadi et al. [25] studied the intrinsic ferromagnetism in Eu and Co co-doped ZnO films. Das et al. [26] reported the paramagnetic nature of in Gd and Mn co-doped ZnO system. Thangeeswari et al. reported RTFM in Bi and Co co-doped ZnO [27]; dysprosium (Dy) and Co co-doped ZnO [28] and Gd and Co co-doped ZnO [29] nanostructures.

In the present study, we report the structural, optical and magnetic properties of Dy and Fe co-doped ZnO nanoparticles. Dy having electron configuration is  $[Xe]4f^{10}6s^2$  and largest value of magnetic moment  $10.63 \mu_B$  among rare earth elements [28], motivated us to choose its co-doping with Fe in ZnO.

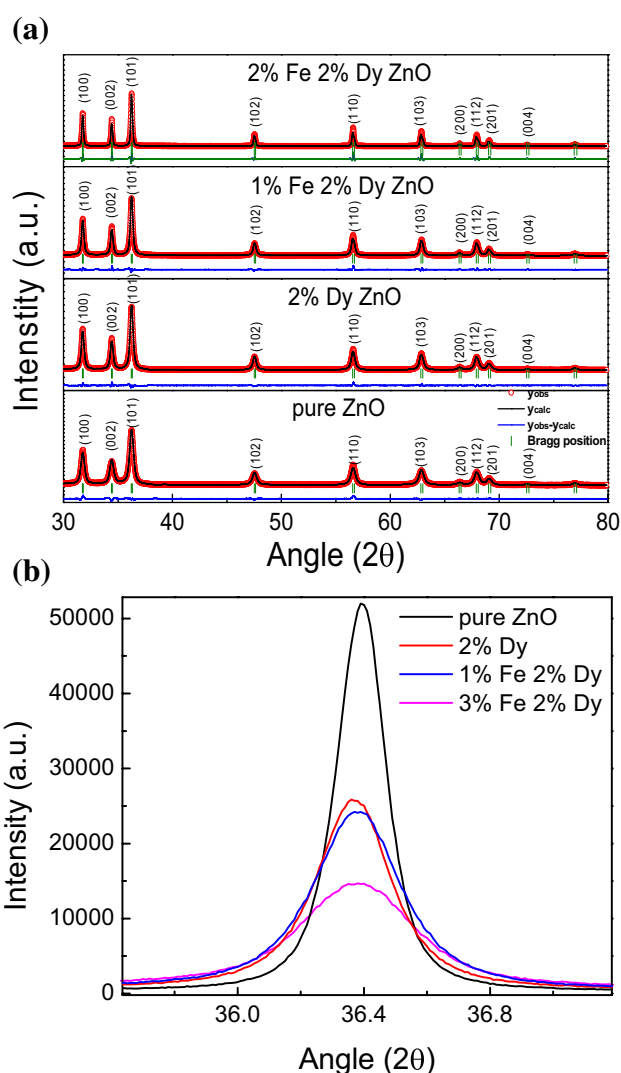
## 2 Experimental

Dy and Fe co-doped ZnO nanoparticles were synthesized using the simple and cost-effective sol–gel method. Zinc acetate, dysprosium nitrate, iron nitrate, monoethanolamine and 2-methoxyethanol were used as the preliminary precursors, stabilizer and solvent, respectively. First, zinc acetate, dysprosium nitrate and iron nitrate were mixed in 2-methoxyethanol. The molar ratio of monoethanolamine to zinc acetate, dysprosium nitrate, iron nitrate was preserved at 1. The resulting mixed solution was stirred for 2 h at 60 °C. Drop by drop, Monoethanolamine was added, during the stirring of mixture resulting in a homogeneous and transparent solution. The sols were aged at room temperature for 24 h and then dried at 300 °C. Subsequently, the products were trodden to get the samples in powder form. Next, these powders were again annealed for 1 h at 500 °C. Afterwards, the annealed products were trodden again to get the nanoparticles.

XRD investigations of the doped ZnO nanoparticles at room temperature were performed using Panalytical X'pert PRO diffractometer. The surface morphological studies of the doped ZnO nanoparticles were made using high resolution transmission electron microscope (HR-TEM) of FEI, USA. The photoluminescence (PL) and Raman studies were performed using Horiba Jobin Yvon LabRAM HR-Evolution spectrometer with a 325 and 532 nm excitation laser, respectively. Magnetic measurements at room temperature were done using 'Quantum Design' vibrating sample magnetometer.

## 3 Results and discussion

Figure 1a presents the Rietveld refined XRD patterns for pure ZnO, Dy doped ZnO and Dy and Fe co-doped ZnO nanostructures attained using the FullProf software. Rietveld refinement was initiated for all the samples using

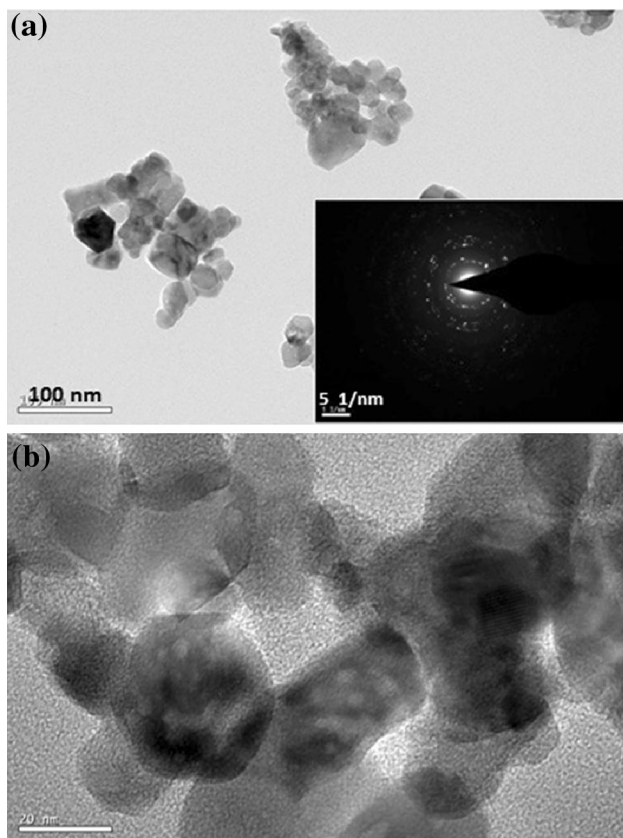


**Fig. 1** **a** Rietveld refined and indexed XRD patterns for sol–gel synthesized pure and doped ZnO nanoparticles. **b** Variation in broadening and intensity for the peak (101) for pure and doped ZnO nanoparticles synthesized using sol–gel technique

Pseudo-Voigt function. Wurtzite structure of ZnO (space group  $P63mc$ ) was chosen as initial model structure during the Rietveld refinement. Calculated parameters for pure ZnO, Dy doped ZnO and Dy and Fe co-doped ZnO nanoparticles using Rietveld refinement were presented in Table 1. XRD investigations depict show that the Dy and Fe co-doping did not alter the host ZnO structure. The highest intensity peak (101) for pure ZnO is observed at  $36.4^\circ$ . The intensity of the same peak for 2% Dy doped ZnO observed is almost half as well as it shifted slightly towards left. The shifting of the same may be due to the higher ionic radii of  $Dy^{3+}$  (91 pm) than that of  $Zn^{2+}$  (74 pm). The intensity of the same degrades because of the defects created by Dy doping. With 1% Fe co-doping it again slightly shifts to the higher side which may be due to smaller ionic radii of

**Table 1** Calculated parameters for doped ZnO nanoparticles from Rietveld refinement

SAMPLE	Lattice parameters (Å)			Cell volume (Å <sup>3</sup> )	R <sub>p</sub>	R <sub>wp</sub>	R <sub>exp</sub>	χ <sup>2</sup>	Crystal- lite size D (nm)
	a	b	c						
Pure ZnO	3.252	3.252	5.209	47.706	6.21	7.41	7.05	1.11	48
2% Dy doped ZnO	3.252	3.252	5.208	47.697	4.64	8.86	4.84	1.8	38.2
1% Fe and 2% Dy co-doped ZnO	3.252	3.252	5.209	47.706	6.51	7.47	4.85	1.62	39.5
2% Fe and 2% Dy co-doped ZnO	3.252	3.252	5.210	47.715	8.25	8.18	5.27	1.5	22.6

**Fig. 2** **a** TEM micrograph for Fe and Dy doped ZnO nanoparticles; inset is showing the SAED pattern for the same **b** HR-TEM micrograph for Fe and Dy doped ZnO nanoparticles

Fe<sup>3+</sup> (64 pm). With 2% Fe co-doping it again shifts slightly towards the right side. With the increase in Fe co-doping, reduction in intensity as well as broadening of diffraction peaks are observed (Fig. 1b). This may be attributed to the decrease in crystalline structure of ZnO with increase in Dy and Fe co-doping.

The crystallite size is found to be in the range 22–48 nm for doped ZnO nanoparticles using Scherrer formula. Figure 2a shows TEM micrograph image of Dy and Fe co-doped ZnO nanoparticles. TEM image clearly presents the slightly dissimilar sizes and shapes of doped ZnO nanoparticles.

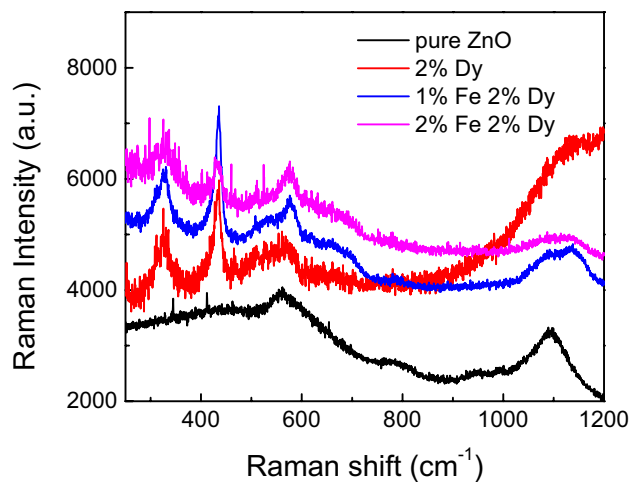
**Fig. 3** Room temperature Raman spectra for sol-gel synthesized pure and doped ZnO nanoparticles

Figure 2b presents the HR-TEM micrograph of the same Dy and Fe co-doped ZnO nanoparticles. It is clearly depicted from high resolution micrograph that most of the nanoparticles are almost spherical in shape. Polycrystalline nature of Dy and Fe co-doped ZnO nanoparticles is clearly validated through selected area electron diffraction (SAED) pattern shown in inset of Fig. 2a. The points having variable intensity as observed in the SAED pattern indicates that the Dy and Fe co-doped ZnO nanoparticles composed of crystallites of different size, in confirmation with the crystallite size (22–48 nm) estimated using Scherrer formula and HR-TEM results.

Group theory suggested that the ZnO having wurtzite structure, relates to the space group C<sub>6v</sub> with 2 formula units per primitive cell each of which further engages C<sub>3v</sub> sites, resulting in 9 optical and 3 acoustic phonon branches [30]. Raman spectra of pure ZnO, Dy doped ZnO and Fe and Dy co-doped ZnO is presented in Fig. 3. E<sub>2</sub>(high) mode [31, 32] of hexagonal ZnO (wurtzite structure) at 437–439 cm<sup>-1</sup> is present in Raman spectra of all samples. A minor transfer in this peak depicts lattice strain produced by the dopant in host ZnO. The peak at 406 cm<sup>-1</sup> attributes to E<sub>1</sub>(TO) modes reveal the potency of the lattice bond. The weak peak

at  $331\text{ cm}^{-1}$  is allocated to  $A_1$  symmetry modes related to multiple phonon scattering processes. The band in the range  $578\text{--}584\text{ cm}^{-1}$  is related to host defects such as zinc interstitials ( $Z_{Ni}$ ) and oxygen vacancies ( $V_o$ ), assigned to the  $E_1(\text{LO})$  mode [31, 33]. The weak peak at  $547\text{ cm}^{-1}$  depicts the inclusion of Dy in the host ZnO, results in generation of additional defects. The uncharacteristic vibrational modes nearly  $509\text{--}522\text{ cm}^{-1}$  are related to defect concentration in the host [33].  $288\text{ cm}^{-1}$  peak in co-doped ZnO may be due to the restricted vibrations of Zn atoms [34]. The peaks at  $564$  and  $1098\text{ cm}^{-1}$  correspond to the  $A_1(\text{LO})$  and  $A_1(2\text{LO})$  modes of the hexagonal ZnO [35]. No Raman signals corresponding to impurity and secondary phase appeared in the doped ZnO spectra.

Figure 4 presents photoluminescence (PL) spectra at room temperature of pure ZnO, Dy doped ZnO and Fe and Dy co-doped ZnO nanoparticles. Room temperature photoluminescence studies show that for pure ZnO, band-edge emission occurs at  $381\text{ nm}$  while for  $2\%$  Dy doped ZnO it shifts to  $383\text{ nm}$ . With  $1\%$  co-doping of Fe in Dy doped ZnO, band-edge emission is observed at  $382\text{ nm}$  while for  $2\%$  Fe co-doped ZnO same is observed at  $380\text{ nm}$ . Replacement of divalent  $Zn^{2+}$  ions with trivalent  $Dy^{3+}$  ions results in crystalline defects in ZnO, such as zinc interstitials ( $Z_{Ni}$ ), zinc vacancies ( $V_{Zn}$ ), oxygen interstitials ( $O_i$ ) and oxygen vacancies ( $V_o$ ) which are in corroboration with Raman results. The broad peak at  $556\text{ nm}$  corresponding to green emission may be attributed to the surface oxygen defects for example singly ionized  $V_o$  and  $O_i$  [36]. These defects result in reduction of UV emission. The peak corresponding to orange-red emission at  $627\text{ nm}$  is usually credited to the  $O_i$  defects [37, 38] and caused due to the transition from conduction band to monovalent vacancies or transition from

interstitial zinc or oxygen vacancy to monovalent vacancies. The peak appeared at about  $768\text{ nm}$  corresponds to near IR emission in ZnO nanoparticles which may be attributed to the surplus interstitial oxygen ( $O_i$ ) and interstitial zinc atoms ( $Z_{Ni}$ ) or may be related to second order ( $383\times 2$ ) UV emission [39, 40]. Fe co-doping in Dy doped ZnO results in quenching of near band-edge emission which may be due to a effective communication among excitons lying in the conduction band and the electrons (photogenerated) with increase in Fe doping. The peak due attributed to green luminescence shows a slight red-shift and its intensity is also reduced with the increase in Fe dopant concentration. This quenching occurs may be due to the trapping of photo generated electrons in the trap centres produced by the  $Fe^{3+}$  ions [41–43].

Magnetic studies of Dy and Fe co-doped ZnO nanoparticles are appealing because of sturdy hybridization of localized  $4f$  electrons with the conduction  $d$  electrons. In comparison to transition metal  $d$  electrons, rare earth  $f$  electrons can pair effectively with the  $s$  electrons (host) which escort to the likelihood of electron intervened ferromagnetism [27–29]. Figure 5 shows M–H curves at room temperature for pure ZnO, Dy doped ZnO and Fe and Dy co-doped ZnO nanoparticles. Inset of the Fig. 5 clearly shows the presence of weak ferromagnetic ordering in all samples. Weak magnetic behavior is observed at low magnetic field for pure ZnO. With increase in the applied magnetic field, diamagnetic behavior comes into the picture.  $2\%$  Dy doped ZnO shows the blend of weak ferromagnetic and paramagnetic behavior.  $1\%$  Fe co-doping in  $2\%$  Dy doped ZnO lowers the magnetic moment, while  $2\%$  Fe co-doping in  $2\%$  Dy doped

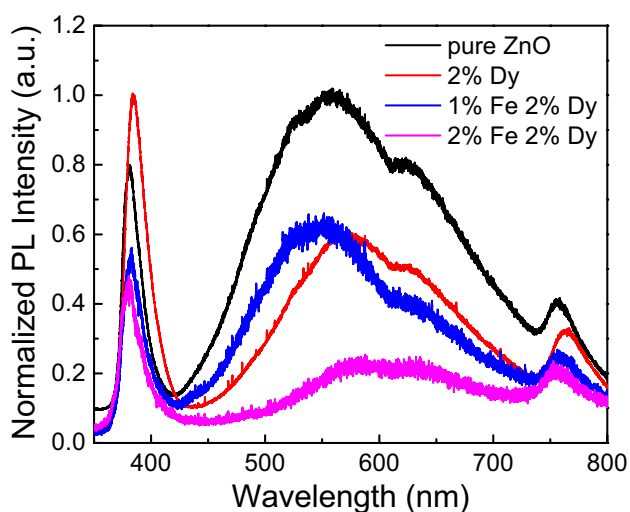


**Fig. 4** Room temperature photoluminescence spectra for sol-gel synthesized pure and doped ZnO nanoparticles

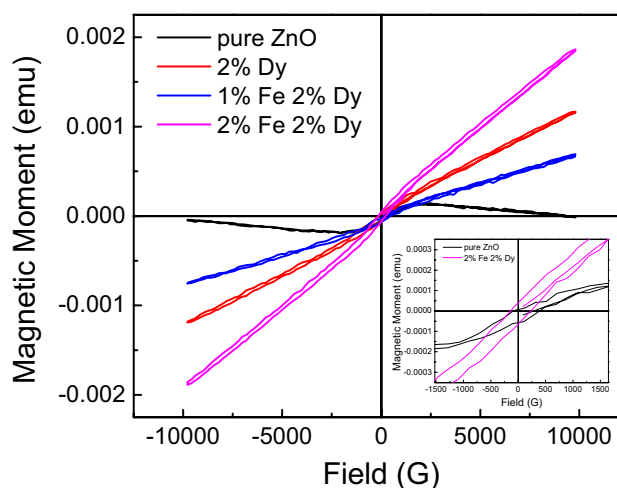


**Fig. 5** Room temperature M–H curves for sol-gel synthesized pure and doped ZnO nanoparticles; inset is showing the magnified view of M–H curves for pure ZnO and  $2\%$  Fe and  $2\%$  Dy co-doped ZnO nanoparticles

ZnO increase the magnetic moment value with antiferromagnetic signature.

It is well reported that the paramagnetic nature in doped ZnO samples originated from the uncorrelated spin of transition metal and rare earth ions [44]. It has been described earlier that the exchange interaction between two neighboring transition metal and rare earth ions are antiferromagnetic in nature [42]. Photongkam et al. [45] reported strong magnetization in Co and Eu co-doped ZnO thin films and further suggested that the sturdy ferromagnetic pairing between localized 3d electrons of  $\text{Co}^{2+}$  and the localized carriers stimulated by  $\text{Eu}^{3+}$  which got trapped in singly ionized oxygen vacancies. Lo et al. [46] claimed that Dy doped ZnO can only be paramagnetic on the basis of experimental results and correlated the same with the reported ab-initio calculations of Dy doped ZnO by El Hachimi et al. [47]. Photoluminescence studies show that with the increase in Fe co-doping, the intensity of green emission peak due to oxygen vacancies decreases resulting in antiferromagnetic behavior. Therefore to enhance ferromagnetic order, the appropriate doping concentration of Dy and Fe in ZnO wurtzite structure is playing a vital role to get an optimum number of charge carriers and oxygen vacancies, which may be useful for spintronics based solid state devices.

## 4 Conclusions

Pure ZnO and Fe and Dy co-doped ZnO nanoparticles have been synthesized using the sol–gel method. XRD patterns depict that the pure, as well as doped ZnO nanoparticles, crystallized in the wurtzite structure exclusive of development of any secondary phase. Room temperature PL and Raman investigations of doped ZnO nanoparticles validate the existence of singly ionized oxygen vacancies which may further results in weak magnetic ordering in the synthesized samples. 2% Dy doped ZnO samples illustrate paramagnetic behavior along with weak ferromagnetic part. Further 2% Fe co-doping in 2% Dy doped ZnO leads to antiferromagnetic behavior with weak ferromagnetic component.

## References

1. F. Matsukura, H. Ohno, A. Shen, Y. Sugawara, *Phys. Rev. B* **57**, R2037 (1998)
2. H. Ohno, *Science* **281**, 951 (1998)
3. J.Y. Kim, J.H. Park, B.G. Park, H.J. Noh, S.J. Oh, J.S. Yang, D.H. Kim, S.D. Bu, T.W. Noh, H.J. Lin, H.H. Hsieh, C.T. Chen, *Phys. Rev. Lett.* **90**, 017401 (2003)
4. A.S. Risbud, N.A. Spaldin, Z.Q. Chen, S. Stemmer, R. Seshadri, *Phys. Rev. B* **68**, 205202 (2003)
5. M.L. Reed, N.A. El-Masry, H.H. Stadelmaier, M.K. Ritums, M.J. Reed, C.A. Parker, J.C. Roberts, S.M. Bedair, *Appl. Phys. Lett.* **79**, 3473 (2001)
6. S.B. Ogale, *Adv. Mater.* **22**, 3125 (2010)
7. G.Z. Xing, Y.H. Lu, Y.F. Tian, J.B. Yi, C.C. Lim, Y.F. Li, G.P. Li, D.D. Wang, B. Yao, J. Ding, Y.P. Feng, T. Wu, *AIP Adv.* **1**, 022152 (2011)
8. G.Z. Xing, J.B. Yi, J.G. Tao, T. Liu, L.M. Wong, Z. Zhang, G.P. Li, S.J. Wang, J. Ding, T.C. Sum, C.H.A. Huan, T. Wu, *Adv. Mater.* **20**, 3521 (2008)
9. E.-Z. Liu, Y. Liu, J.Z. He, *Appl. Phys. Lett.* **93**, 132506 (2008)
10. D. Kim, J. Yang, J. Hong, *J. Appl. Phys.* **106**, 013908 (2009)
11. B. Chen, Q.X. Yu, Q.Q. Gao, Y. Liao, G.Z. Wang, *Appl. Phys. Lett.* **102**, 132405 (2013)
12. A. Kaushik, B. Dalela, R. Rathore, V.S. Vats, B.L. Choudhary, P.A. Alvi, S. Kumar, S. Dalela, *J. Alloys Compd.* **578**, 328 (2013)
13. J.A. Wibowo, N.F. Djaja, R. Saleh, *Adv. Mater. Phys. Chem.* **3**, 48 (2013)
14. S. Kumar, C.L. Chen, C.L. Dong, Y.K. Ho, J.F. Lee, T.S. Chan, R. Thangavel, T.K. Chen, B.H. Mok, S.M. Rao, M.K. Wu, *J. Mater. Sci.* **48**, 2618 (2013)
15. P. Kaur, S.K. Pandey, S. Kumar, N.S. Negi, C.L. Chen, S.M. Rao, M.K. Wu, *Appl. Nano* **5**, 975 (2015)
16. P.P. Murmu, J. Kennedy, B.J. Ruck, G.V.M. Williams, A. Markwit, S. Rubanov, A.A. Suvorova, *J. Mater. Sci.* **47**, 1119 (2012)
17. S. Kumar, P. Kaur, C.L. Chen, R. Thangavel, C.L. Dong, Y.K. Ho, J.F. Lee, T.S. Chan, T.K. Chen, B.H. Mok, S.M. Rao, M.K. Wu, *J. Alloys Compd.* **588**, 705 (2014)
18. S. Kumar, R. Thangavel, *Elec. Mater. Lett.* **13**, 129 (2017)
19. P. Kaur, S. Kumar, C.L. Chen, Y.Y. Hsu, T.S. Chan, C.L. Dong, C. Srivastava, A. Singh, S.M. Rao, *Appl. Phys. A* **122**, 1 (2016)
20. Z.F. Wu, K. Cheng, F. Zhang, R.F. Guan, X.M. Wuc, L.J. Zhuge, *J. Alloys Compd.* **615**, 521 (2014)
21. S. Chattopadhyay, T.K. Nath, A.J. Behan, J.R. Neal, D. Score, Q. Feng, A.M. Fox, G.A. Gehring, *J. Magn. Magn. Mater.* **323**, 1033 (2011)
22. L. Liu, P.Y. Yu, Z. Ma, S.S. Mao, *Phys. Rev. Lett.* **100**, 127203 (2008)
23. Q. Xu, H. Schmidt, H. Hochmuth, M. Lorenz, A. Setzer, P. Esquinazi, C. Meinecke, M. Grundmann, *J. Phys. D: Appl. Phys.* **41**, 105012 (2008)
24. M.H.N. Assadi, Y.B. Zhang, P. Photongkam, S. Li, *J. Appl. Phys.* **109**, 013909 (2011)
25. H. Huang, Y. Ou, S. Xu, G. Fang, M. Li, X.Z. Zhao, *Appl. Surf. Sci.* **254**, 2013 (2008)
26. J. Das, D.K. Mishra, D.R. Sahu, B.K. Roul, *Physica B* **407**, 3575 (2012)
27. T. Thangeeswari, J. Velmurugan, M. Priya, *J. Mater. Sci. Mater. Electron.* **24**, 4817 (2013)
28. T. Thangeeswari, P. Murugasen, J. Velmurugan, *J. Supercond. Nov. Magn.* **28**, 2505 (2015)
29. T. Thangeeswari, M. Priya, J. Velmurugan, *J. Mater. Sci. Mater. Electron.* **26**, 2436 (2015)
30. R. Thangavel, R.S. Moirangthem, W.S. Lee, Y.C. Chang, P.K. Wei, J. Kumar, *J. Raman Spectrosc.* **41**, 1594 (2010)
31. A. Umar, E.K. Suh, Y.B. Hahn, *Solid State Commun.* **139**, 447 (2006)
32. X.X. Lin, Y.F. Zhu, W.Z. Shen, *J. Phys. Chem. C* **113**, 1812 (2009)
33. Y.C. Tseng, Y.J. Lin, H.C. Chang, Y.H. Chen, C.J. Liu, Y.Y. Zou, *J. Lumin.* **132**, 1896 (2012)
34. X. Zhu, H.Z. Wu, D.J. Qiu, Z. Yuan, G. Jin, J. Kong, W. Shen, *Opt. Commun.* **283**, 2695 (2010)
35. S.J. Chen, Y.C. Liu, Y.M. Lu, J.Y. Zhang, D.Z. Shen, X.W. Fan, *J. Cryst. Growth* **289**, 55 (2006)
36. S. Pyne, G.P. Sahoo, D.K. Bhui, H. Bar, P. Sarkar, S. Samanta, A. Maity, A. Misra, *Spectrochim. Acta A* **93**, 100 (2012)
37. X.L. Wu, G.G. Siu, C.L. Fu, H.C. Ong, *Appl. Phys. Lett.* **78**, 2285 (2001)

38. X. Xiu, X. Wu, H. Cao, R.P.H. Chang, *J. Appl. Phys.* **95**, 3141 (2004)
39. R.B.M. Cross, M.M. De Souza, E.M.S. Narayan, *Nanotechnology* **16**, 2188 (2005)
40. T. Mahalingam, K.M. Lee, K.H. Park, S. Lee, Y. Ahn, J.Y. Park, K.H. Koh, *Nanotechnology* **18**, 035606 (2007)
41. M.V. Limaye, S.B. Singh, R. Das, P. Poddar, S.K. Kulkarni, *J. Solid State Chem.* **184**, 391 (2011)
42. N.S. Norberg, K.R. Kittilstved, J.E. Amonette, R.K. Kukkadapu, D.A. Schwartz, D.R. Gamelin, *J. Am. Chem. Soc.* **126**, 9387 (2004)
43. S.Y. Kuo, W.C. Chen, F.I. Lai, C.P. Cheng, H.C. Kua, S.C. Wang, W.F. Hsieh, *J. Cryst. Growth* **287**, 78 (2006)
44. S. Das, S. Das, D. Das, S. Sutradhar, *J. Alloys Compd.* **691**, 739 (2017)
45. P. Photongkam, Y.B. Zhang, M.H.N. Assadi, S. Li, D. Yu, *J. Appl. Phys.* **107**, 033909 (2010)
46. F.Y. Lo, Y.C. Ting, K.C. Chou, T.C. Hsieh, C.W. Ye, Y.Y. Hsu, M.Y. Chern, H.L. Liu, *J. Appl. Phys.* **117**, 213911 (2015)
47. A.G. El Hachimi, H. Zaari, A. Benyoussef, M. El Yadari, A. El Kenz, *J. Rare Earths* **32**, 715 (2014)